Computer Vision and Image Understanding 000 (2016) 1–18

Contents lists available at ScienceDirect

Computer Vision and Image Understanding

journal homepage: www.elsevier.com/locate/cviu

Automatic large-scale three dimensional modeling using cooperative multiple robots

Ryo Kurazume[a,*], Souichiro Oshima[a], Shingo Nagakura[a], Yongjin Jeong[a], Yumi Iwashita[b]

[a] Kyushu University, 744 Motooka, Nishi-ku, Fukuoka 8190395, Japan
[b] Jet Propulsion Laboratory, M/S 198-235 4800, Oak Grove Drive Pasadena, 91109 CA, USA

ARTICLE INFO

Article history:
Received 28 October 2015
Revised 11 May 2016
Accepted 16 May 2016
Available online xxx

Keywords:
Laser measurement
Multiple robots
3D modeling
Automatic sensing planning

ABSTRACT

3D modeling of real objects by a 3D laser scanner has become popular in many applications, such as reverse engineering of petrochemical plants, civil engineering and construction, and digital preservation of cultural properties. Despite the development of lightweight and high-speed laser scanners, the complicated measurement procedure and long measurement time are still heavy burdens for widespread use of laser scanning. To solve these problems, a robotic 3D scanning system using multiple robots has been proposed. This system, named CPS-SLAM, consists of a parent robot with a 3D laser scanner and child robots with target markers. A large-scale 3D model is acquired by an on-board 3D laser scanner on the parent robot from several positions determined precisely by a localization technique, named the Cooperative Positioning System (CPS), that uses multiple robots. Therefore, this system can build a 3D model without complicated post-processing procedures such as ICP. In addition, this system is an open-loop SLAM system and a very precise 3D model can be obtained without closed loops. This paper proposes an automatic planning technique for a laser measurement by using CPS-SLAM. Planning a proper scanning strategy depending on a target structure makes it possible to perform laser scanning efficiently and accurately even for a large-scale and complex environment. The proposed technique plans an efficient scanning strategy automatically by taking account of several criteria, such as visibility between robots, error accumulation, and efficient traveling. We conducted computer simulations and outdoor experiments to verify the performance of the proposed technique.

1. Introduction

Due to the development of low-cost laser measurement systems such as FARO Focus 3D, Leica Scanstation, and TOPCON GLS-1500, laser measurement has become popular in recent years in many applications such as reverse engineering of petrochemical plants, civil engineering and construction, or digital preservation of cultural properties.

For acquiring a whole 3D model of a large-scale architecture, multiple laser scans have to be performed repeatedly around the target architecture. Then the obtained partial range data are aligned precisely by predefined markers or data points themselves by Iterative Closest Point (ICP) or Normal Distribution Transform (NDT) algorithms. Despite the development of lightweight and high-speed laser scanners, the complicated measurement procedure, long measurement time, and post-processing procedure are still heavy burdens for the widespread use of laser scanning.

To solve these problems, a robotic 3D scanning system, named CPS-SLAM (cooperative positioning system - simultaneous localization and mapping), has been proposed for scanning a large-scale architecture (Kurazume et al., 2009). This system consists of a parent robot and child robots. The parent robot is equipped with a 3D laser measurement device such as a total station, and the child robots are equipped with target markers. For localizing the parent robot, the child robots keep a stand-still state and act as landmarks. Next, the parent robot stops and acts as a landmark for localizing the child robots. By using the laser measurement device and the target markers, the robot positions are determined with high accuracy of land surveying. Since the parent and child robots move in coordination to localize each other, we call this system the cooperative positioning system (CPS) (Kurazume et al., 1994). Moreover, laser scanning is performed repeatedly by the laser scanner mounted on the parent robot at a number of

* Corresponding author.
E-mail addresses: kurazume@ait.kyushu-u.ac.jp (R. Kurazume), Yumi.Iwashita@jpl.nasa.gov (Y. Iwashita).

http://dx.doi.org/10.1016/j.cviu.2016.05.008

locations whose positions are determined precisely by CPS. The obtained range data are aligned by using the position information directly without applying ICP or NDT algorithms. We performed a number of measurement experiments at the Dazaifu Tenmangu shrine in Japan and tunnel shape measurements at construction sites (Kurazume et al., 2009; Tobata et al., 2012).

In conventional 3D laser scanning, the Next Best View (NBV) problem, which plans the best scanning positions to capture a whole 3D model efficiently, is quite important to reduce the measurement time and scanning cost. However, in actual use, the scanning strategy is often determined by the operator's experience and intuition. Although the NBV problem is quite important even in the CPS-SLAM system, the scan planning is also usually determined manually. Therefore, efficiency and optimality have not been considered qualitatively and explicitly, and thus, in some cases, the measurement time tends to become longer since some regions are overlapped unexpectedly or unnecessary movements are planned.

This paper proposes a solution of the NBV problem for the laser measurement system by using multiple robots (Oshima et al., 2015). We consider the visibility between robots, the suppression of error accumulation, and efficient robot movements in order to develop an automatic planning technique of a large-scale architecture for CPS-SLAM. Furthermore, we verify the performance of the proposed automatic planning method through a number of computer simulations in various environments, and indoor and outdoor experiments using two types of machine models, CPS-VII and CPS-VIII.

2. Related work

The optimum design of the positions of sensors, which are utilized, for example, in security camera systems, has been studied for many years in the fields of computational geometry and computer vision (Mavrinac and Chen, 2013; Newman and Jain, 1995; Tarabanis et al., 1995). See Robin and Lacroix (2016) for a detailed survey.

In general, this problem can be categorized into two categories: the geometry of an environment and/or a target object is known, or the geometry is not known. In the case that geometrical information is available, the problem of optimum sensor positions, which minimizes blind regions in a surveillance area or efficient appearance inspection planning, have been considered. Especially, an optimum layout problem of sensors (observers) in an indoor environment is called an "art gallery problem" and has been studied in the field of computer science (Aggarwal, 1984; O'Rourke, 1987). Stamos and Allen (1998) proposed an interactive layout planning system to reduce blind regions. Topcuoglu et al. (2011) showed a technique for a wide topological map that realizes an optimum sensor layout and the confidentiality of sensors at the same time. Chen and Li (2004) and Scott et al. (2001) proposed some optimum observation planning techniques of an object with a known shape. They achieved high efficiency and high accuracy by using a 3D range sensor. Prieto et al. (1999) discussed optimum inspection planning for an object by using CAD data and a range sensor with high accuracy.

For a cooperative surveillance using multiple robots have also been discussed so far. Nilsson et al. (2008) proposed a polynomial time algorithm for camera positioning problem for surveillance using UGVs (Unmanned Ground Vehicle) equipped with cameras. They solved two kinds of tasks, the first is how to create a line-of-sight perimeter around a given set of buildings and the second is how to achieve good stationary coverage of a give set of walls. Geng et al. (2013) proposed the surveillance planning approach for a group of UAVs (Unmanned Aerial Vehicle) consisting of two stage approach is proposed. In the first stage, vantage set, which is a set of camera locations for complete visibility coverage of the target area, is generated. In the second stage, the vantage set are divided for each UAV and flying paths for continuous surveillance are generated. In both stages, the Genetic Algorithm is applied to search for an optimal solution. Tokekar and Isler (2014) formulated discussed Δ-guarding problem, which is the extension of the conventional art gallery problem to take into account self-occlusion caused by a person or an object in an environment. To guarantee to be seen from at least one guard in spite of self-occlusion, they presented an approximation algorithm which uses at most 12 times the optimal number of guards.

On the other hand, for an object with unknown geometrical information, observation planning techniques for shape measurement (Chen and Li, 2005; Li and Liu, 2005; Marchand and Chaumette, 1997; Papadopoulos-Orfanos and Schmitt, 1997; Zha et al., 1997) and active recognition systems utilizing sensor motions (Aloimonos, 2013; Bajcsy, 1988) have been proposed. Okamoto et al. (1998) proposed a fundamental scheme for the NBV problem. Their scheme uses a stochastic observation model and probabilistic sensor fusion technique to determine a proper observation location. As another solution of the NBV problem, Li and Liu (2005) utilized information entropy to describe the uncertainty of an observation model and selected the optimum location at which the acquired information is expected to be maximized.

Active SLAM (or SPLAM, Simultaneous Planning Localization and Mapping) (Carlone et al., 2010; Leung et al., 2006; Sim, 2005; Stachniss et al., 2004) is a technique to actively control a robot to explore unknown area effectively and completely while minimizing the pose uncertainty in SLAM framework. Accuracy and coverage of the map are considered as a map uncertainty. To reduce the pose uncertainty, active loop closing is achieved according to the uncertainty of pose estimation. Sim (2005) proposed a technique using Voronoi graph and dummy landmarks in unexplored area to ensure the coverage of the environment. Pose uncertainty is described by EKF for bearings-only SLAM. Leung et al. (2006) proposed an efficient algorithm to reduce both uncertainties of the map and the pose efficiently using Model Predictive Control (MPC) with attractors. MPC and attractors control the robot behavior considering the local and global constraints, respectively. Carlone et al. (2010) discussed to minimize both uncertainties in a framework of Rao-Blackwellized Particle filter. Appropriate robot behavior is adaptively selected by evaluating the posterior approximation using Kullback–Leibler divergence. Carrillo et al. (2015) investigated how the uncertainty is increased according to some criteria in the exploration phase. In many techniques in Active SLAM including above, greedy technique (optimize only with respect to the next time step) is adopted. Therefore, global optimization is hard to be achieved. Atanasov et al. (2015) proposed a non-greedy multi-robot active SLAM which guarantees the performance using a square-root information filter.

On the other hand, some techniques assume that accurate robot position can be obtained, and find the optimum strategy to explore unknown area effectively. One of the traditional techniques is the frontier-based approach (Konolige et al., 2006; Stachniss et al., 2004; Yamauchi, 1997). In this technique, the boundaries between known and unknown areas, which is called frontier, are selected as potential target positions for exploration.

Although the technique proposed in this paper belongs to the frontier-based approach under the condition of unknown geometrical information, we consider both the exploration and the pose uncertainties. Since CPS-SLAM utilizes the CPS for the localization of multiple robots, as described below, the accuracy of the pose estimation is considerably much improved compared with laser-based or odometry-based approaches. However, to ensure the preciseness of the pose estimation, we have to consider some strong restrictions, such as the robots must have lines of sight to each other while exploring. Therefore, we introduce a Visibility graph to

Please cite this article as: R. Kurazume et al., Automatic large-scale three dimensional modeling using cooperative multiple robots, Computer Vision and Image Understanding (2016), http://dx.doi.org/10.1016/j.cviu.2016.05.008

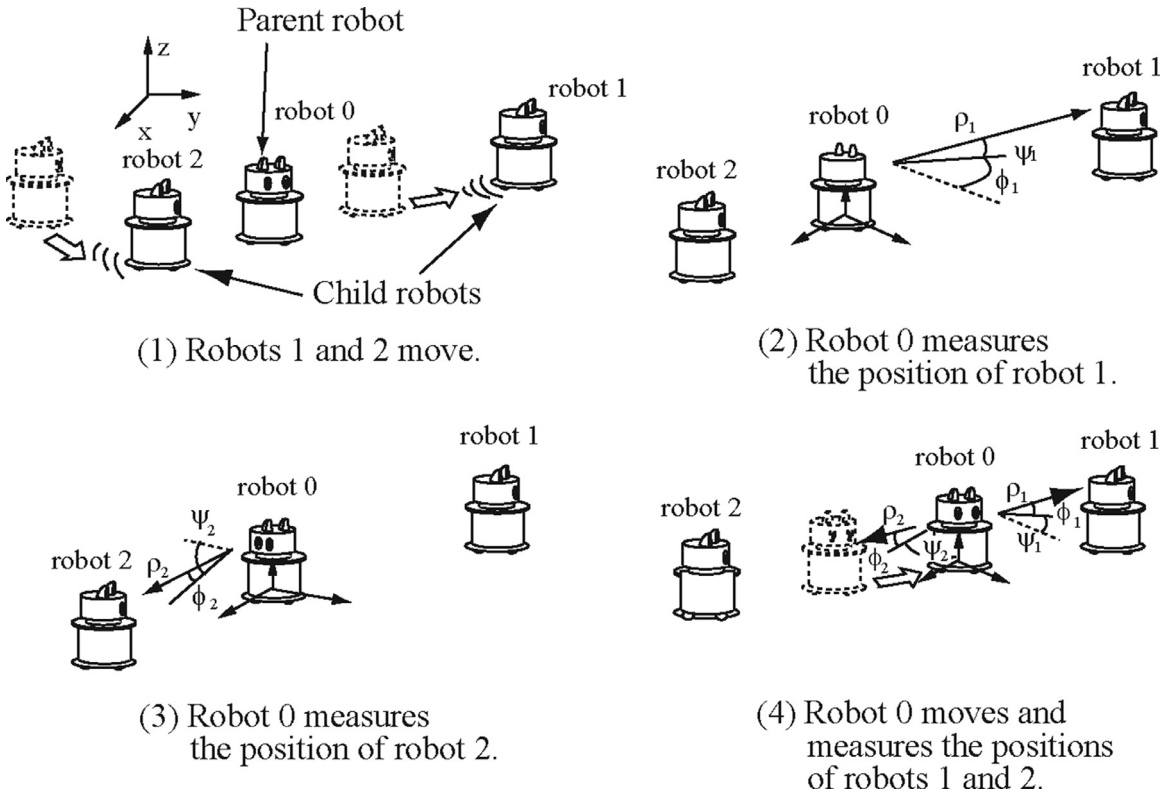

Fig. 1. Cooperative positioning system, CPS.

a frontier-based approach to satisfy both of Active SLAM and keeping visibility. Consequently, the proposed approach is quite different from the above mentioned conventional problems, in which the view position can be chosen freely.

As mentioned in Section 1 , we proposed the fundamental idea of the corporative positioning technique using multiple robots in Kurazume et al. (1994). Although this is the key technique in the present paper, we did not mention about the 3D scanning in Kurazume et al. (1994). In Kurazume et al. (2009), Tobata et al. (2012), and Jeong et al. (2012), we proposed the 3D scanning system based on the proposed cooperative positioning system, which can be summarized as follows:

- In Kurazume et al. (2009) and Tobata et al. (2012), CPS-V and indoor/outdoor experiments were presented. The accuracy was 0.24 % of the distance traveled, which means the error is 0.22 m after the robot moved 93.9 m in an indoor environment Kurazume et al. (2009). On the other hand, in a large-scale outdoor environment, the accuracy was 0.091 % of the distance traveled, which means the error is 0.494 m after the robot moved 543.4 m Tobata et al. (2012).
- In Jeong et al. (2012), CPS-V and CPS-VI were presented for a tunnel shape measurement system. The accuracy was 0.037 % of the distance traveled, which means the error is 0.0296 m after the robot moved 80.0 m.

However, in all these systems, the scanning strategies were planned by human operators, and thus an optimum solution for efficient scanning procedure was not considered.

In Oshima et al. (2015), we proposed an automatic planning technique for CPS-VII which is also presented in the present paper. However, following points are newly discussed in the present paper.

- In Oshima et al. (2015) we discussed about the planning technique for CPS-VII which has two child robots. On the other hand, the planning technique for CPS-VIII is also discussed in the present paper. We rearranged the whole procedures again and explained them for CPS-VII and CPS-VIII separately and clearly. The difference of CPS-VII and CPS-VIII are as follows: (1) two wheeled child robots are used for CPS-VII and four or more wheeled robots and quadcopters are used for CPS-VIII, and (2) the sensors are replaced from a total station and the SICK 2D laser scanner to the FARO 3D laser scanner. Owing to these changes, the accuracy is drastically improved. As shown in Section 5.5, the accuracy for CPS-VIII is 0.0085 % of the distance traveled, which means the error is 0.0231 m after the robot moved 270.1 m. In addition, some of the child robots can move with the parent robot at the same time owing to the redundancy. This makes the total measurement time of CPS-VIII much shorter than CPS-VII.
- To improve the reliability of the discussion, new simulations and experiments were conducted such as the comparison with manual operation (Fig. 26), the comparison for three types of environments in Fig. 13 by simulations (Fig. 6), and new outdoor experiments (Fig. 23).

3. Laser measurement system using multiple robots for a large-scale architecture, CPS-SLAM

This paper proposes an observation planning technique for the laser measurement system, CPS-SLAM using multiple robots (Jeong et al., 2012; Kurazume et al., 2009; Oshima et al., 2015; Tobata et al., 2012). In this system, the positions of parent and child robots are determined by CPS. Fig. 1 shows the fundamental strategy of CPS, which consists of a parent robot 0 equipped with a laser measurement device (e.g., total station) and two child robots 1 and 2.

First, the parent robot 0 is stopped at a known position. Then, the following procedure is repeated.

(1) Move child robots 1 and 2 and stop them.

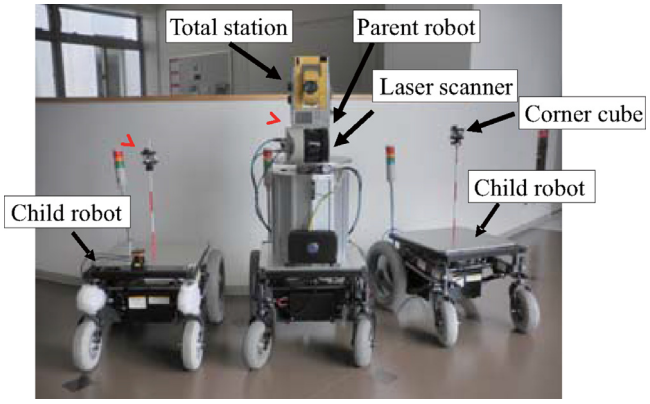

Fig. 2. CPS-SLAM machine model, CPS-VII.

(2) Measure the distance and the azimuth and elevation angles from the parent robot 0 to child robot 1 by the laser measurement device and calculate the position of child robot 1.
(3) Determine the position of child robot 2 in the same manner.
(4) Move the parent robot while child robots 1 and 2 are stopped.
(5) Measure the distance and direction to the child robots and determine the position of the parent robot 0.

In CPS-SLAM, the parent robot is equipped with a laser scanner in addition to the laser measurement device, and scans the target object from multiple locations that are localized precisely by CPS. The obtained partial range data are transformed to the world coordinate frame by using the position information and aligned precisely with simple algebra. No post-processing procedures such as ICP or NDT are required to obtain a large-scale model.

Obviously, it is possible to use the geometrical information with the above technique. We have already evaluated the accuracy in case that we combined the proposed CPS technique (target-based) and ICP (point cloud-based) in Tobata et al. (2012) and verified that the accuracy was improved if the accuracy of CPS is low. However, in general, as adopted by typical land-surveying procedures, the target-based approach is more accurate and reliable than the point cloud-based approach if the enough number of stationary targets are utilized since the ambiguity of the point distribution can be avoided explicitly.

In the proposed CPS-SLAM, the error is accumulated as the robot travels. To suppress the error accumulation, we need some fixed targets (child robots) which can be observed before and after the movements and solve a loop-closure problem. It is also possible to combine the point cloud-based technique to correct an accumulated error. However, we think that the error accumulation of the proposed technique is much smaller than the conventional SLAM approaches without loop-closure as shown by the following experiments.

We have been developing several CPS machine models. Some of them are introduced in the following sections.

3.1. The seventh CPS-SLAM system (CPS-VII)

Fig. 2 shows the seventh CPS-SLAM machine model (CPS-VII) consisting of a parent robot and two child robots. The parent robot is equipped with a total station (TOPCON, GPT-9005A) and a laser scanner (SICK, LMS 511), and the child robots are equipped with omni-directional corner cubes. Fig. 3 shows the total station and the omni-directional corner cube. The total station searches and finds the omni-directional corner cube automatically, and measures the distance and azimuth and elevation angles to it very precisely. We repeated measurement experiments in outdoor and indoor environments and confirmed that the accuracy of the CPS-VII is 0.034 % (3D error is 116 mm after the parent robot moved 343 m) to 0.054 % (3D error is 98 mm for 181 m) of the total travel distance of the parent robot (Jeong et al., 2012). Fig. 4 shows an example of the obtained 3D model of a large-scale building.

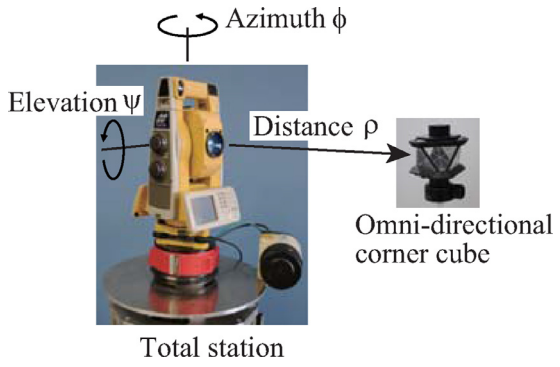

Fig. 3. Total station and corner cube.

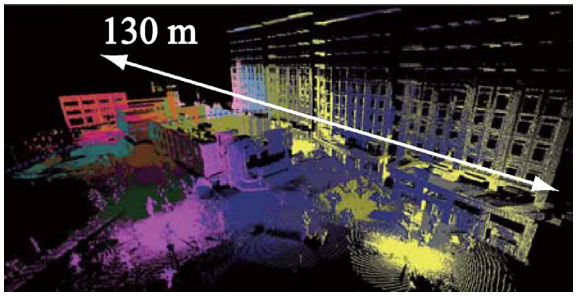

Fig. 4. 3D model of a large building.

Positioning and scanning strategies are shown in Fig. 5. The positioning and scanning are sequentially performed by a total station and a laser scanner, respectively, on the parent robot.

3.2. The eighth CPS-SLAM system (CPS-VIII)

We are developing the new CPS-SLAM system named CPS-VIII shown in Fig. 6. This system consists of a parent robot equipped with a laser scanner (Focus 3D, FARO) and several child robots, including wheeled robots and quadcopters. The child robots hold lightweight white balls as markers instead of corner cubes.

Positioning and scanning strategies are shown in Fig. 7. In contrast to CPS-VII, positioning and scanning are simultaneously performed by a laser scanner mounted on the parent robot. In Fig. 6, a total of five child robots are shown. In this paper, we discuss the CPS-VIII system with four child robots for simplicity.

4. Automatic planning technique

To realize automatic scan planning, we have to consider several conditions, such as efficiency of the laser measurement, reliability to obtain solutions in any situation, suppression of error accumulation and travel distance, and collision avoidance between robots and environment.

In the proposed technique, we assume that several scans have been performed and a set of partial data of the environment have been obtained. The problem is how we choose the NBV in this situation. The strategy of the proposed technique is as follows: First, we extract several candidate locations at which most of the new geometric data will be acquired, and then choose the best location among them considering the distance and error accumulation to reach each location.

Please cite this article as: R. Kurazume et al., Automatic large-scale three dimensional modeling using cooperative multiple robots, Computer Vision and Image Understanding (2016), http://dx.doi.org/10.1016/j.cviu.2016.05.008

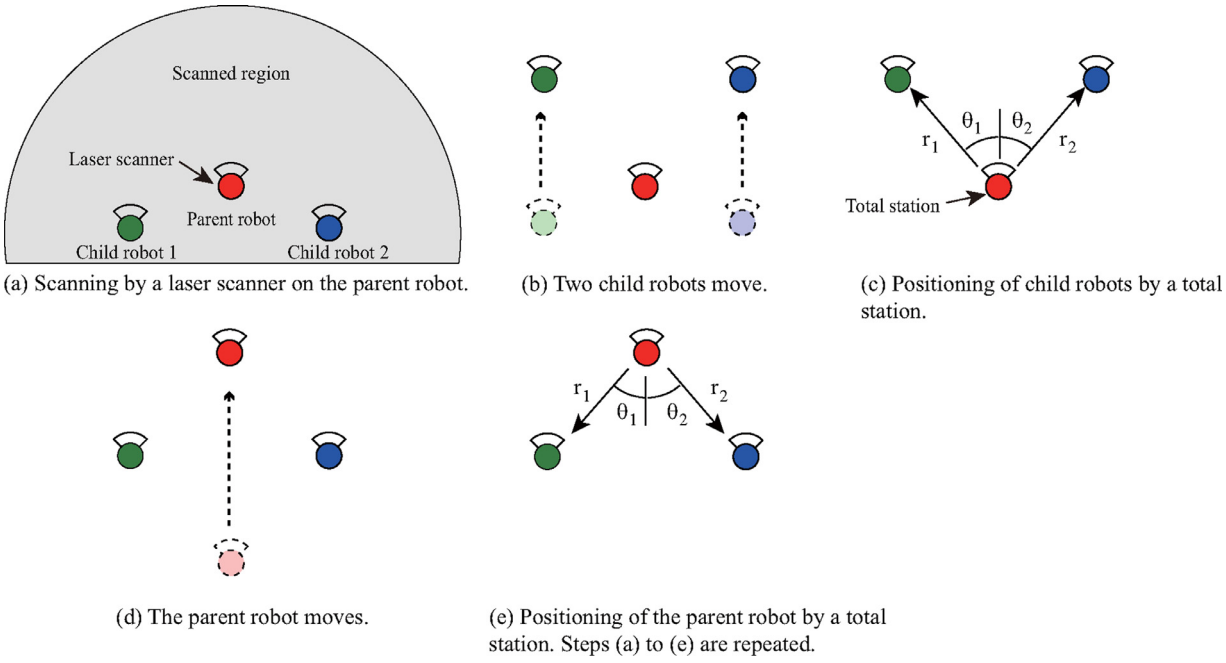

(a) Scanning by a laser scanner on the parent robot. (b) Two child robots move. (c) Positioning of child robots by a total station.

(d) The parent robot moves. (e) Positioning of the parent robot by a total station. Steps (a) to (e) are repeated.

Fig. 5. Positioning and scanning strategies for CPS-VII: positioning and scanning are performed by a total station and a laser scanner, respectively.

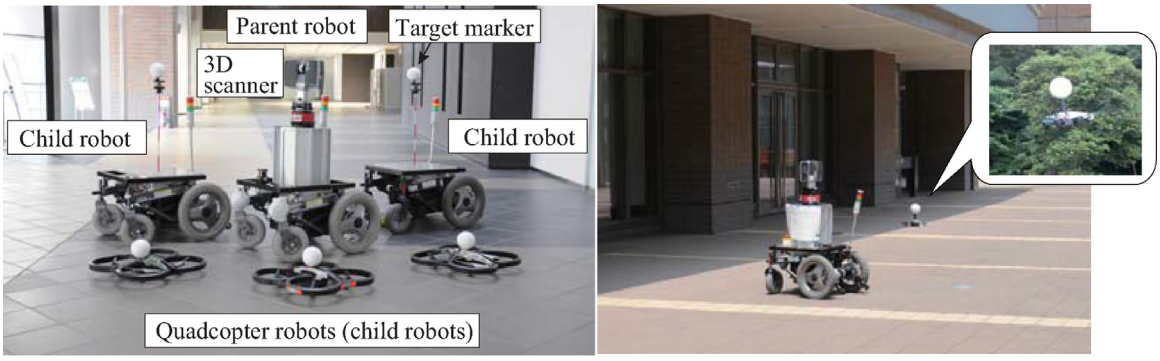

(a) CPS-VIII (b) Target balls on quadcopters

Fig. 6. The 8th CPS machine model, CPS-VIII.

The visibility condition between parent and child robots must be satisfied in CPS-SLAM since the robots must be able to observe each other for the localization. However, this condition is quite hard to satisfy in some cases, especially in a complex environment.

Therefore, in the case that the visibility condition cannot be satisfied, the proposed technique adopts subgoal retrieval by using the Visibility Graph (de Berg et al., 1997), in which new subgoal positions are sequentially retrieved from the final goal position toward the start position by dividing the total trajectory into several short paths. The overview of the proposed technique is shown in Fig. 8.

In the following sections, we introduce the details of the proposed technique separately, as follows.

1. Automatic planning of the target position for the parent robot
2. Automatic planning of the target positions for the child robots

Note that we consider the planning problem in 2D space. To do so, the obtained 3D geometrical data are first transformed to a 2D grid map.

4.1. Automatic planning of target positions for the parent robot

When we design the measurement locations for the parent robot in partially measured environments, we adopted the frontier-based approach (Yamauchi, 1997). In this technique, the following conditions should be considered.

1. The new scanning position should be close to the border areas between known regions that have already been measured by the laser scanner and unknown regions that have not been measured.
2. The new scanning position should be placed far enough from walls or pillars to avoid collision.
3. The new scanning position should be close to the current position.
4. The newly scanned region should be as large as possible.

However, if the environment is large and all the border areas are considered to be candidates, the planning cost will become quite large. Therefore, we adopt the two-step strategy described in the following section. Briefly speaking, we first extract several candidate positions. Then, the optimum position that satisfies the conditions mentioned above is selected.

Please cite this article as: R. Kurazume et al., Automatic large-scale three dimensional modeling using cooperative multiple robots, Computer Vision and Image Understanding (2016), http://dx.doi.org/10.1016/j.cviu.2016.05.008

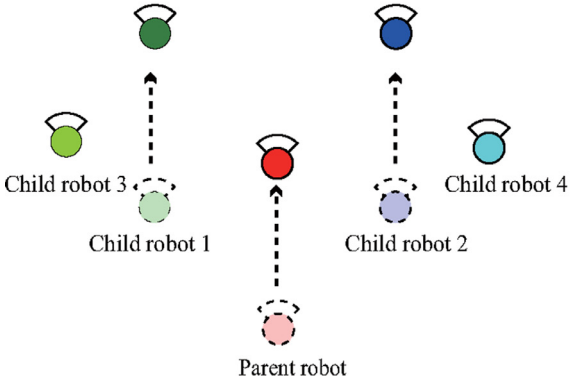

(a) CPS-VIII: The parent robot and two child robots out of four robots move.

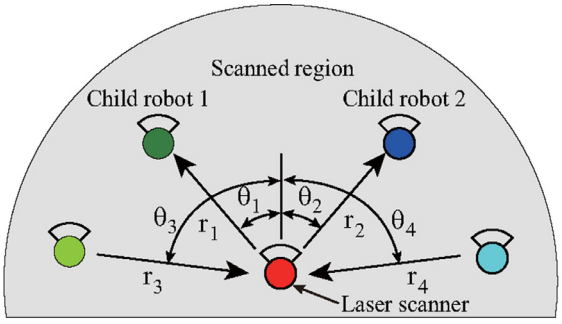

(b) Scanning and positioning of the parent robot and two child robots (1, 2) by a laser scanner using stationary child robots (3,4).

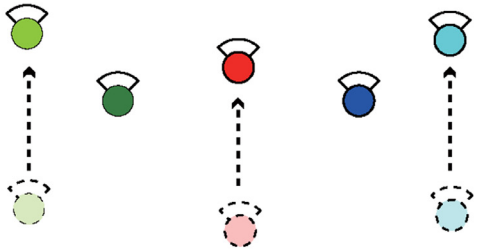

(c) The parent robot and two child robots out of four robots move.

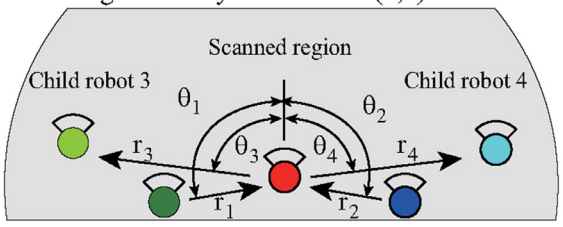

(d) Scanning and positioning of the parent robot and two child robots (3, 4) by a laser scanner using stationary child robots (1,2).

Fig. 7. Positioning and scanning strategies for CPS-VIII: positioning and scanning are performed by a laser scanner simultaneously.

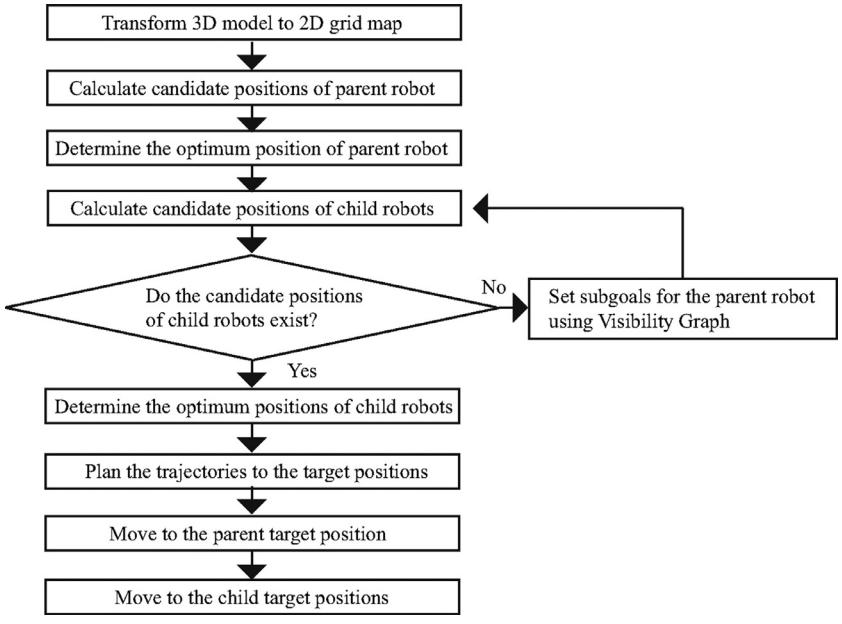

Fig. 8. Flowchart of the automatic planning algorithm.

Please cite this article as: R. Kurazume et al., Automatic large-scale three dimensional modeling using cooperative multiple robots, Computer Vision and Image Understanding (2016), http://dx.doi.org/10.1016/j.cviu.2016.05.008

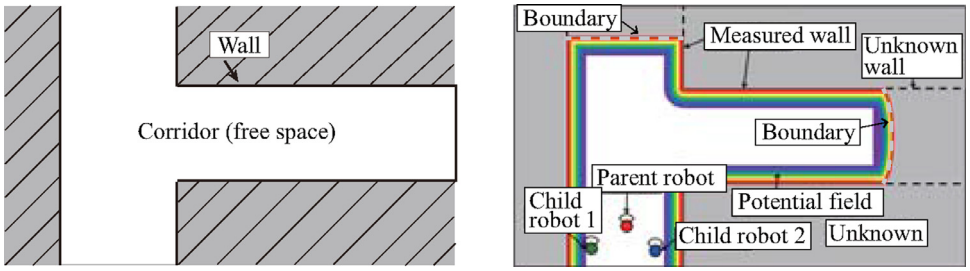

Fig. 9. Left: problem definition. White and gray regions are free and occupied spaces. Right: white region is a measured free space. Detected walls and boundaries between the measured and unknown regions are shown in solid and dotted red lines. Colored lines show the potential field. (For interpretation of the references to color in this figure legend, the reader is referred to the web version of this article.)

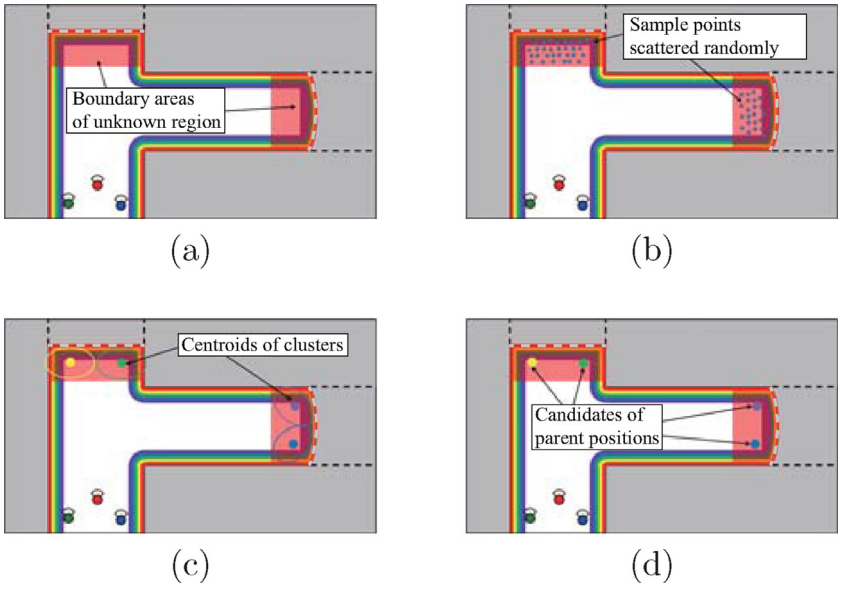

Fig. 10. Determined candidate positions for the parent robot by K-means clustering.

4.1.1. Initial selection of candidate positions

To extract several candidate positions in the border areas, the K-means clustering technique is applied. Figs. 9 and 10 show the problem setting and the extraction procedure, respectively. The detailed procedure is as follows:

(1) Find border lines between known (measured) and unknown (not measured) regions.
(2) Scatter candidate points uniformly in the border area where the distance to the border line is less than a threshold value.
(3) Apply clustering to the candidate points in Step 2.
(4) Select the centroids of each cluster as candidates of the target points of the parent robot.

Note that the number of clusters is determined adaptively according to the size of the border area. In addition, other subsampling techniques such as MAT (medial axis transform) or discrete sampling can be applied.

4.1.2. Determination of target position from candidate positions

Next, we determine the final target position from the candidate target positions based on the conditions listed in Section 4.1. To choose an optimum target position that satisfies all the conditions mentioned above, the following value is evaluated for each candidate target point.

$$G = R \cdot (P^{-1} + \alpha L^{-1} + \beta \cdot S) \quad (1)$$

where G is the evaluated value of each candidate target point, R is a constant value of 0 (unknown or inaccessible) or 1 (known and accessible) that shows the grid condition of the candidate target point, P is the potential value (inverse of distance from the closest obstacle), L is the travel distance from the current parent position, S is the size of an expected newly scanned area in unknown regions where no geometrical information has been obtained so far, and α and β are weights of terms. To calculate S, we assume that no objects other than the ones that have been measured until now exist in the environment. Then we count the number of grids that can be seen from the candidate target position directly without being blocked by obstacles and that are located within the maximum range of the laser scanner, except for the areas scanned previously. We choose the position with the maximum evaluation value among the candidate target positions as the final target position of the parent robot.

4.2. Automatic planning of target positions for the child robots

The target positions of the child robots have to be seen from both the final target position and the initial position of the parent robot, since positioning with CPS is impossible if obstacles exist between the parent and the child robots and the robots do not have lines of sight to each other. In this paper, we call a region from where both the initial and target parent positions are visible as the "AND region" (Fig. 11).

The candidate target positions of the child robots are determined in this AND region according to the following conditions.

Please cite this article as: R. Kurazume et al., Automatic large-scale three dimensional modeling using cooperative multiple robots, Computer Vision and Image Understanding (2016), http://dx.doi.org/10.1016/j.cviu.2016.05.008

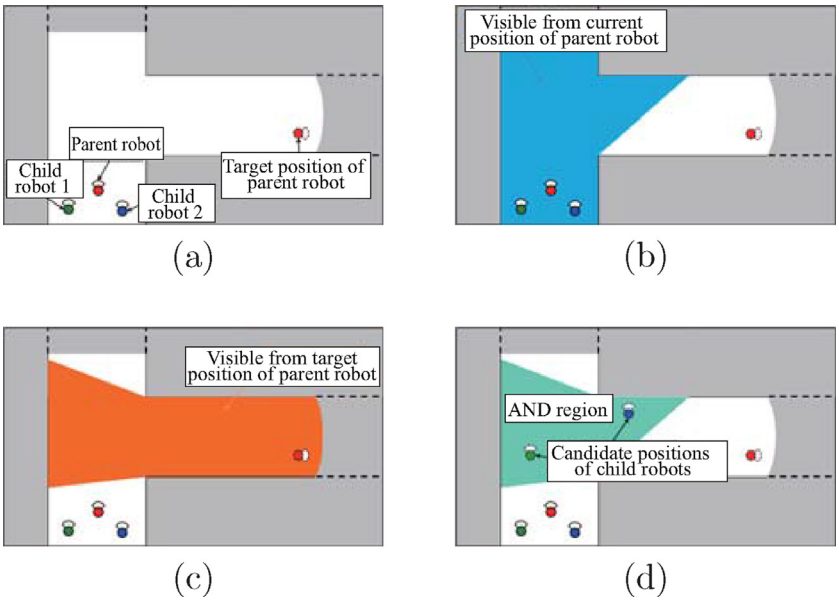

Fig. 11. AND region and candidate positions for child robots.

(1) The candidate position must be located in the AND region and reached from the current child position.
(2) The candidate position must be distant from obstacles.
(3) The distance from the parent robot is less than a threshold.
(4) The relative angle between two child robots from the parent robot is close to 90 degrees.

Here, (3) is established due to the performance of the laser measurement device and (4) is set based on the fact that error accumulation in CPS is most suppressed if the relative angles of the child robots are close to 90 degrees (Kurazume and Hirose, 1998).

As mentioned in Section 3, CPS-VII and CPS-VIII take different strategies. Thus, we explain the procedures for CPS-VII and CPS-VIII separately in the following sections.

4.2.1. CPS-VII

To select the candidate positions of the child robots that satisfy the conditions mentioned above, the following value is calculated at every grid in the AND regions to find the optimum positions of two child robots with the maximum values at the same time.

$$G_c = P^{-1} + \alpha_c \cdot \min(|\theta - \theta_t|^{-1}, \delta_\theta) + \beta_c \cdot \min(|D - D_t|^{-1}, \delta_D) \quad (2)$$

where G_c is the evaluated value of each candidate target point, P is the potential value (inverse of distance from the closest obstacle), θ is the relative angle between the two child robots, D is the distance from the target position of the parent robot, θ_t (= 90 degrees), D_t, δ_θ, and δ_D are constant values, and α_c and β_c are weights of terms. If the current position of the child robot is located in the AND region, we do not determine the next position and keep the child robot at the current position.

4.2.2. CPS-VIII

Since two child robots out of four robots keep stationary for the next localization in Fig. 7(a), we first choose these two child robots (called here as l and m) that satisfy the conditions mentioned above. To do so, the following value G_{c1} is calculated for each child robot in the AND regions and two child robots that have small values are selected as stationary robots.

$$G_{c1} = P^{-1} + \alpha_c \cdot \min(|\theta - \theta_t|^{-1}, \delta_\theta) + \beta_c \cdot \min(|D - D_t|^{-1}, \delta_D) \quad (3)$$

After choosing two stationary robots, the target positions of the other two robots are determined to satisfy the following conditions.

(1) The candidate position must be located in the observable region of the laser scanner on the parent robot and reached from the current child position.
(2) The candidate position must be distant from an obstacle.
(3) The candidate positions should be scattered as much as possible, since the next moving direction of the parent robot is unknown and thus the child robots should be distributed equally to be prepared for any moving directions at the next iteration.

To choose the target position that satisfies these conditions, the following value G_{c2} is calculated in the observable area of the parent robot, and the position that maximizes the value G_{c2} is selected.

$$G_{c2} = P^{-1} + \gamma_c \cdot (D_l + D_m + D_c)^{-1} \quad (4)$$

where D_l and D_m are the distances from the target position of the child robot to the child robots (l and m) that remain stopped, D_c is the distance from the target position to the other child robot that moves at the same time, and γ_c is a weight term.

4.3. Subgoal retrieval using visibility graph

In some cases in the procedure for determining the target position of the child robot mentioned above, proper candidate positions that satisfy the visibility condition cannot be obtained. For example, if the target position of the parent robot is very far from the current position of the child robot and the child robot must pass though several corners to reach there, the AND region, in which both the current and target positions of the parent robot can be seen directly, does not exist. In these cases, we adopt subgoal retrieval using the Visibility Graph, (de Berg et al., 1997). In subgoal retrieval, new subgoal positions of the parent robot are sequentially retrieved from the final goal position to the start position by dividing the total trajectory into several short paths.

The Visibility Graph is a graph representation of all the accessible paths connecting the vertices of the obstacles in the environment. Fig. 12 shows an example of a Visibility Graph. By applying

Please cite this article as: R. Kurazume et al., Automatic large-scale three dimensional modeling using cooperative multiple robots, Computer Vision and Image Understanding (2016), http://dx.doi.org/10.1016/j.cviu.2016.05.008

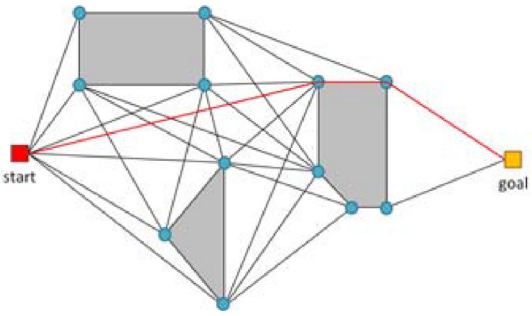

Fig. 12. Example of a visibility graph. The red line is the shortest path connecting the start and end positions. (For interpretation of the references to color in this figure legend, the reader is referred to the web version of this article.)

graph search algorithms, the shortest trajectory between the current and the target positions can be obtained. In this graph representation, each line connecting the vertices indicates that both vertices can be seen from each other. Therefore, if all the robots travel along such lines, the robots have lines of sight of each other and thus the CPS procedure is executable. Due to this fact, we can definitely obtain trajectories to move from the current parent position to the target parent position by using CPS.

The detailed procedure for subgoal retrieval using the Visibility Graph is shown as follows:

(1) Confirm whether the AND region exists between the current and target positions of the parent robot.
(2) If no AND region exists, create the Visibility Graph and find the shortest trajectory.
(3) Retrieve one subgoal for the parent robot along the shortest trajectory from the target position in the Visibility Graph. The subgoals are corner points on the shortest path, which are shown by dots in Fig. 12.
(4) Calculate the AND region between the current robot position and the subgoal.
(5) If the AND region exists, find the target positions of the child robot by using Eqs. (2) or (3).
(6) If the AND region does not exist, retrieve a new subgoal along the shortest trajectory that is one step closer to the current parent robot position.
(7) Repeat Steps 4–6 until the AND region exists.
(8) Set the subgoal as the current parent position and repeat Steps 4–7 until the parent robot reaches the target position.

4.4. Safe robot movement along Voronoi edge

As mentioned above, the robots can move from the initial position to the final target position along the edges connecting the subgoals in the Visibility Graph. However, since the subgoals are set on the vertexes of obstacles, the obtained trajectories pass close to the obstacles. To obtain safer trajectories, we calculate the Voronoi diagram (Aurenhammer, 1991) and set the Voronoi edges as actual trajectories. The robots move first to the nearest position on the Voronoi edges from the initial position, move along the Voronoi edges, and leave from the Voronoi edges to the final target position.

5. Computer simulations and experiments

5.1. Computer simulations

We next evaluate the performance of the proposed technique by computer simulations for the CPS-VII system. In this simulation, we prepare several 2D grid maps with 800 × 600 grids (Maps A, B, and C) or 1116 × 856 grids (Map D) as unknown environments, as shown in Fig. 13, and start scans from several initial positions selected randomly. The grid size is 0.1 m × 0.1 m for each map. We set the maximum range of the omni-directional laser scanner on the parent robot to 20 m. Note that, although the structure of the environment is designed before starting the simulation, the robots do not have any knowledge about the environment at the beginning, and the measurement strategy is planned based on the map, which is gradually expanded as the scans are repeated. Examples of the planned trajectories of three robots for Map A are shown in Fig. 14.

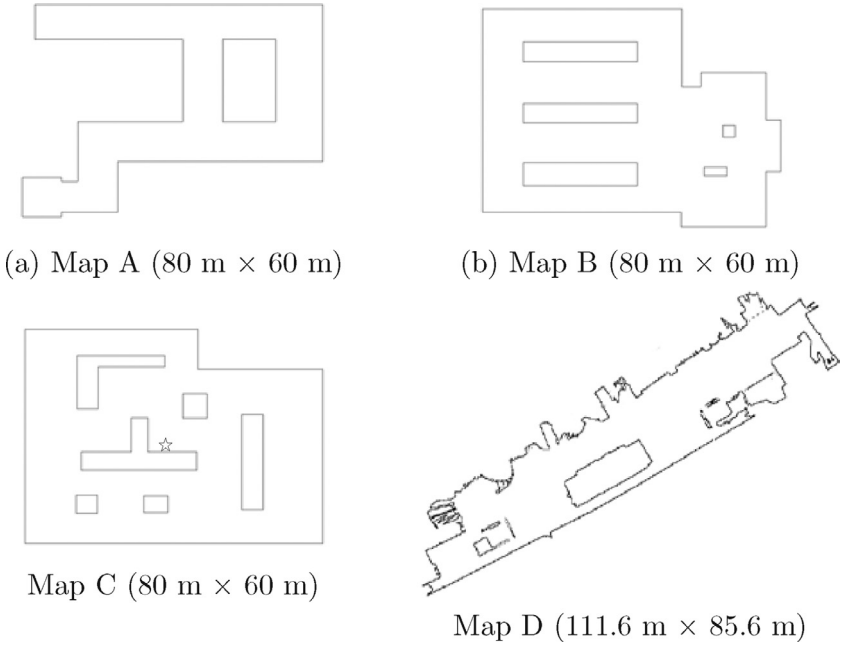

Fig. 13. Examples of the environments (Maps A, B, C, and D).

Please cite this article as: R. Kurazume et al., Automatic large-scale three dimensional modeling using cooperative multiple robots, Computer Vision and Image Understanding (2016), http://dx.doi.org/10.1016/j.cviu.2016.05.008

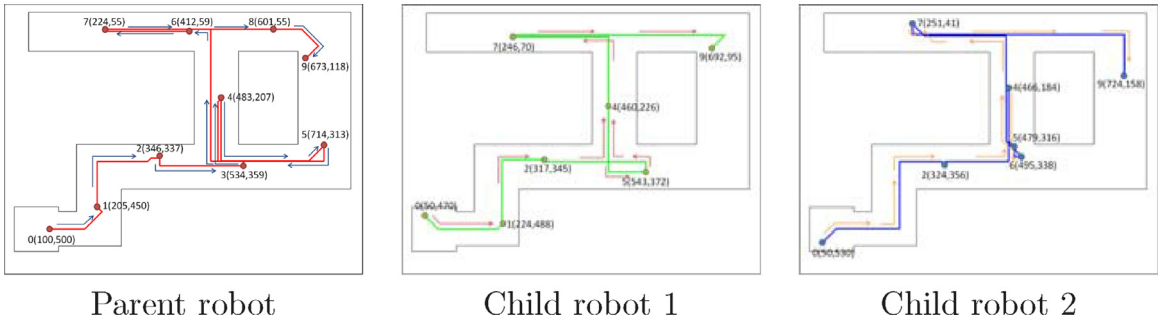

Fig. 14. Planned trajectories of parent and child robots for Map A.

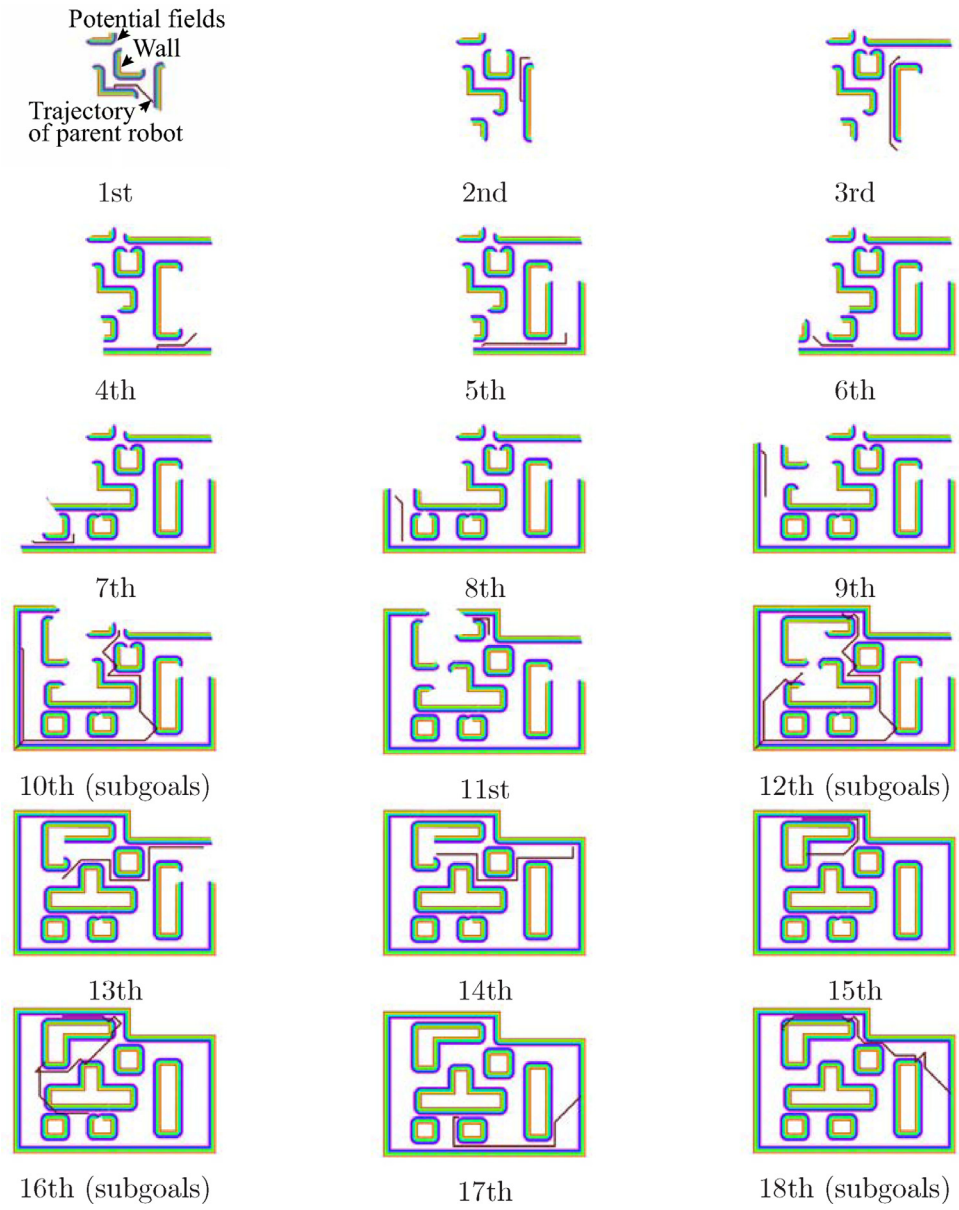

Fig. 15. Measured map and trajectories of parent robot in the case that the target position maximizing the newly scanned area is selected ($\alpha = 0$) for Map C.

5.1.1. Planning of target positions for the parent robot

We verified the performance of the planning technique for the target positions of the parent robot proposed in Section 4.1 by changing parameters α and β in Eq. (1). We adopted the following two simulation conditions.

(a) Select the paths that make the expected newly scanned areas S in unknown regions as large as possible ($\alpha = 0$).
(b) Select the paths that make the travel distance L of the parent robot as small as possible ($\beta = 0$).

Please cite this article as: R. Kurazume et al., Automatic large-scale three dimensional modeling using cooperative multiple robots, Computer Vision and Image Understanding (2016), http://dx.doi.org/10.1016/j.cviu.2016.05.008

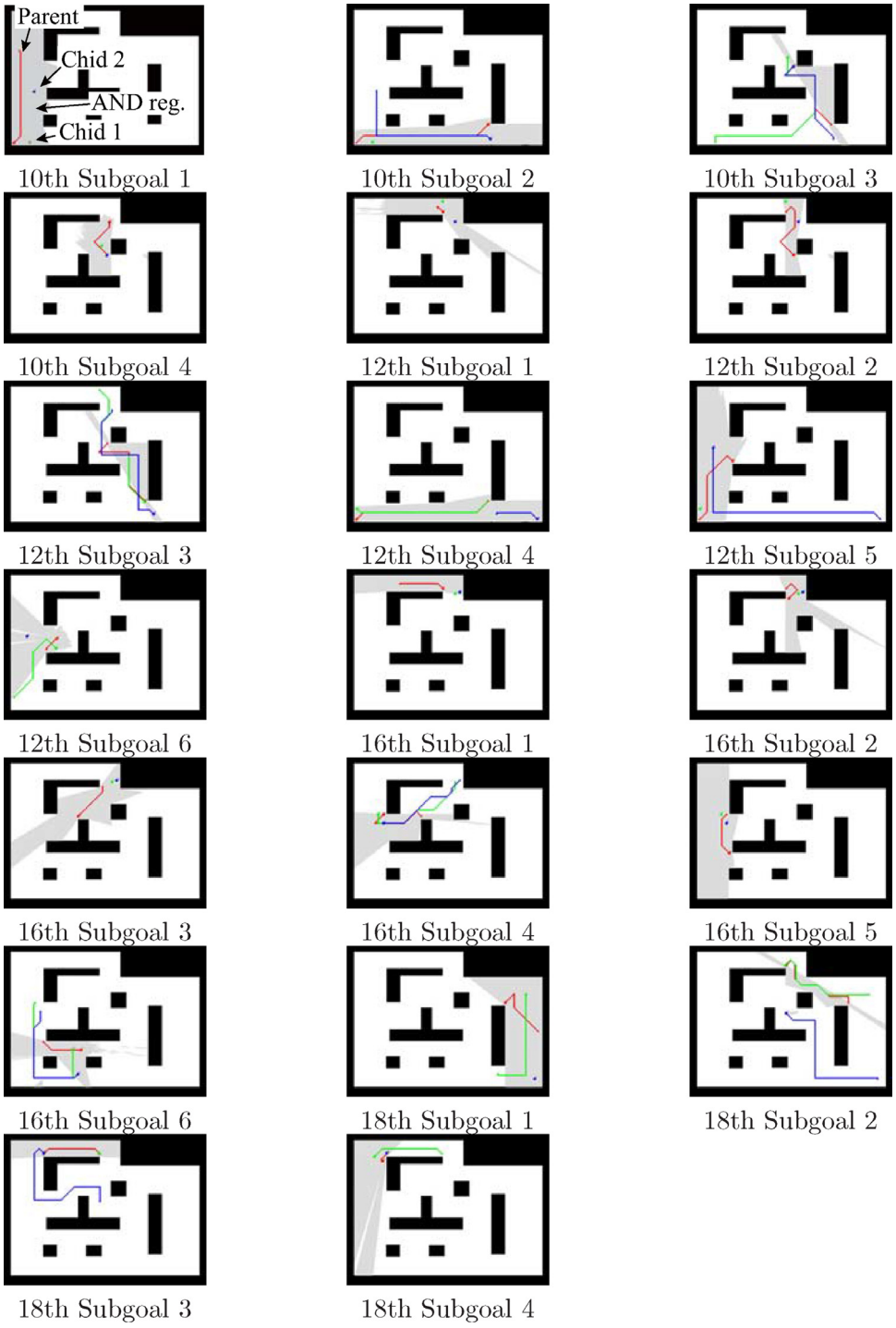

Fig. 16. Subgoals in the case of $\alpha = 0$ (10th, 12th, 16th, and 18th measurements).

As examples, we show the measured maps of Map C acquired sequentially for cases (a) and (b) in Figs. 15 and 17, respectively. Fig. 16 illustrates the subgoal retrieval for case (a) in Fig. 15. In these examples, the initial position of the parent robot is indicated by the star in Fig. 13.

From Fig. 17, we can see that the target positions close to the previous positions are selected and the subgoal retrieval is not performed in this condition ($\beta = 0$), since the selected target positions are all visible from the previous positions. However, the newly scanned areas at each scanning are small and thus the number of scans becomes large. In this simulation, we need to scan 23 times to obtain a whole map. On the other hand, if we choose the parent target positions that maximize the expected newly scanned areas S in unknown regions ($\alpha = 0$), the subgoal retrievals are performed at the 10th, 12th, 16th, and 18th measurements, as shown in Fig. 16, since the distance to the target position is not considered and invisible target positions tend to be selected. Meanwhile, the number of required scannings to obtain the map of whole regions becomes small and planning is terminated at the 18th scanning. We also can see that the trajectories of the parent robot for each movement are longer in the case of $\alpha = 0$ in Fig. 15 than in the case of $\beta = 0$ in Fig. 17.

Please cite this article as: R. Kurazume et al., Automatic large-scale three dimensional modeling using cooperative multiple robots, Computer Vision and Image Understanding (2016), http://dx.doi.org/10.1016/j.cviu.2016.05.008

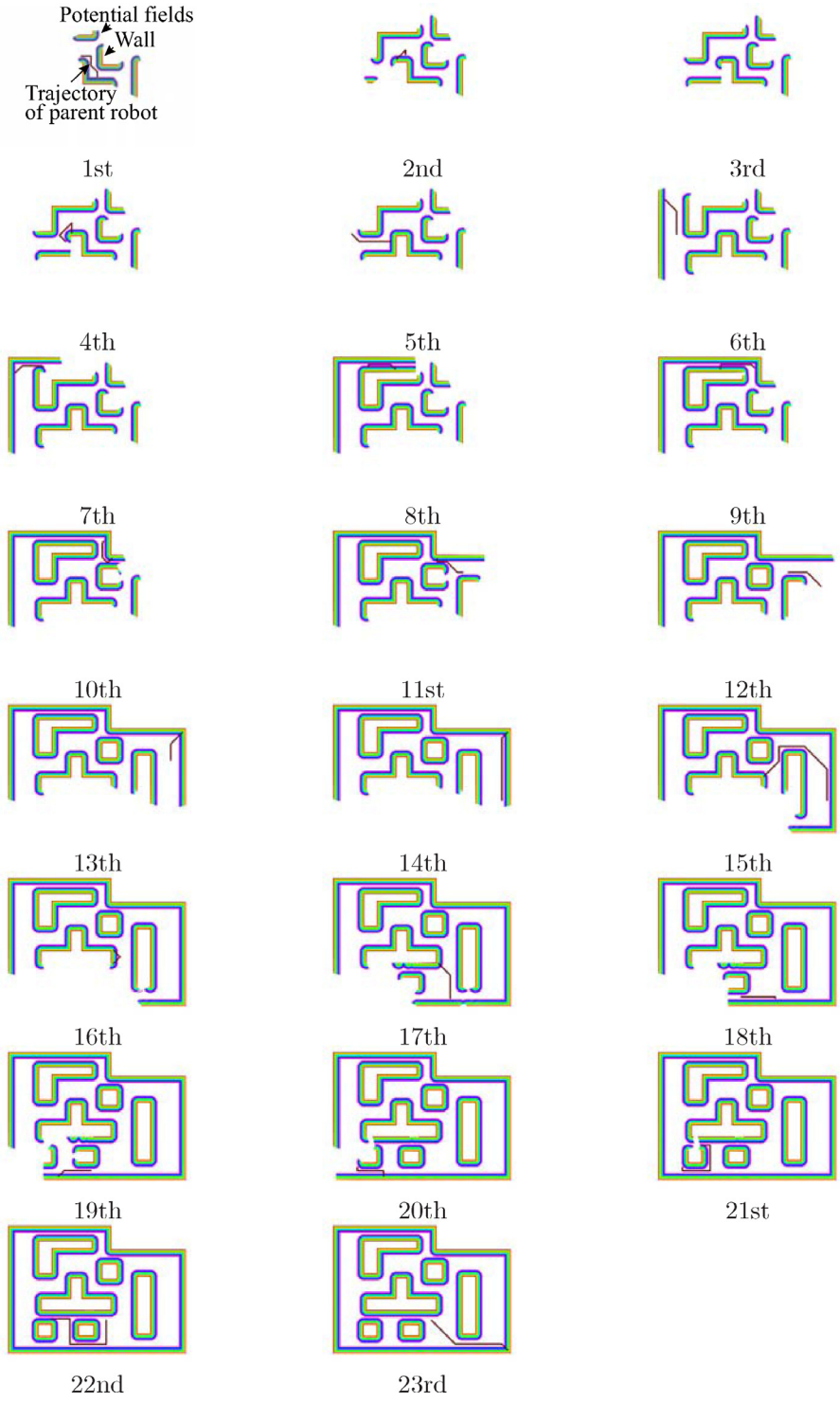

Fig. 17. Measured map and trajectories of parent robot in the case that the closest target position is selected ($\beta = 0$) for Map C.

Moreover, Fig. 18 shows the total travel distance (the horizontal axis includes subgoal retrievals) and the area coverage rate (the horizontal axis does not include subgoal retrievals) for cases (a) (newly scanned areas S in unknown regions are large, $\alpha = 0$) and (b) (distance of movement of the parent robot is small, $\beta = 0$). The average of the five trials of manual planning by a human operator is also plotted. From these figures, we can see that, in case (b), although the total travel distance becomes short, the number of measurements becomes large and the increasing area coverage rate (gradient of Fig. 18(b)) is 5.46 [%/measurement]. On the other hand, in case (a), although the total travel distance becomes long, the number of measurements becomes small and the increasing area coverage rate is 6.14 [%/measurement]. In the case of manual operation, both the total travel distance and the number of measurements become large, and the increasing area coverage rate is 5.02 [%/measurement] for an average of five trials. Furthermore, the increasing area coverage rates per travel distance are 0.232 %/m for case (a), 0.430 %/m for (b), and 0.331 %/m for the manual operation. Therefore, the efficiency of the measurement of case (b) could be improved by 30.2 % by our proposed technique in comparison

Please cite this article as: R. Kurazume et al., Automatic large-scale three dimensional modeling using cooperative multiple robots, Computer Vision and Image Understanding (2016), http://dx.doi.org/10.1016/j.cviu.2016.05.008

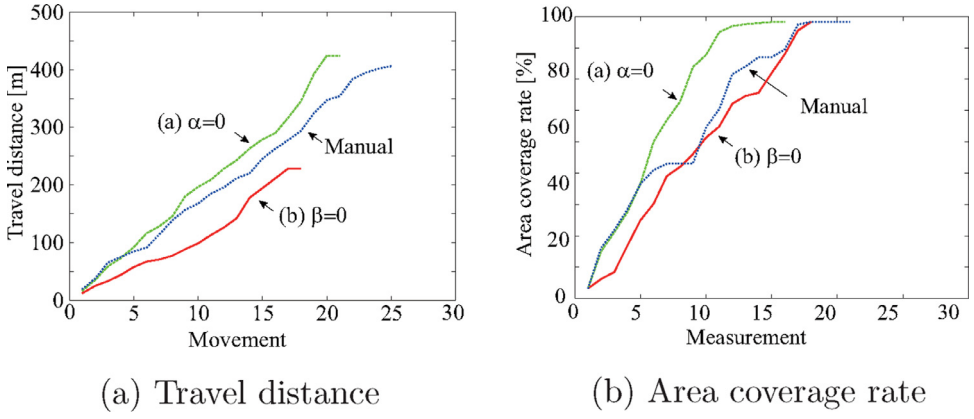

Fig. 18. Comparison of travel distance and measured area of the parent robot.

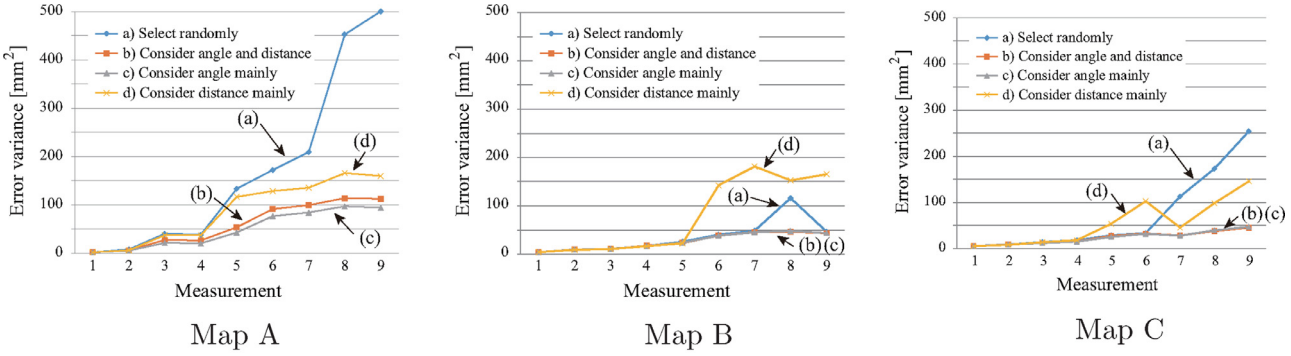

Fig. 19. Comparison of positioning errors.

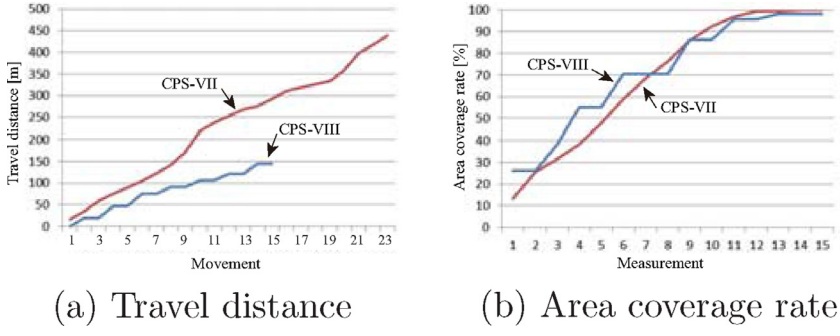

Fig. 20. Comparison of the area coverage rate and total travel distance of the parent robot for Map C.

with the manual operation. In addition, the number of measurements when the area coverage rate exceeds 98 % is 16 for case (a), 18 for case (b), and 19.6 for the manual operation. Case (b) decreases the number of measurements by 18.4 % by our proposed technique in comparison with the manual operation.

The parameters α and β are very environment dependent. Since it is not possible to estimate the optimum parameters beforehand, on-line adaptation is required. One simple approach to adapt them to the environment on-line is that the behavior of the robots is changed according to the distribution of the frontiers (border areas). For example, if there are many frontiers around the current robot position, the robot should concentrate to investigate these areas by decreasing β, and vice versa.

5.1.2. Planning of target positions for the child robots

To evaluate the performance of the planning technique, which suppressed the error accumulation of the child robots as proposed in Section 4.2, we carried out computer simulations by changing the parameters α_c and β_c in Eq. (2) and compared the accumulated errors. The simulation conditions to be compared are as follows:

(a) Select child robot positions randomly.
(b) Set $\alpha_c \simeq \beta_c$.
(c) Set $\alpha_c \gg \beta_c$.
(d) Set $\alpha_c \ll \beta_c$.

Condition (a) determines the positions of the child robots randomly without Eq. (2) so that the positioning is valid for CPS. Condition (c) determines the positions so that the relative angle between the child robots becomes as close to 90 degrees as possible, and condition (d) determines the positions so that the relative distance between the parent and child robots becomes $D_t (= 3\,\mathrm{m})$. The accumulated error is calculated theoretically by the fundamental equation of error propagation in Kurazume and Hirose (1998). In the simulation we adopted $\alpha = 0.01$ and $\beta = 0.001$ so that the

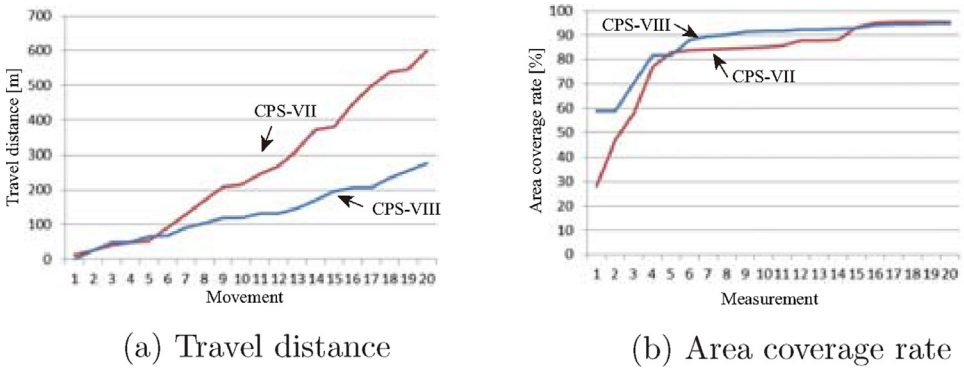

Fig. 21. Comparison of the area coverage rate and total travel distance of the parent robot for Map D.

Fig. 22. Photo of outdoor environment and CPS-VII.

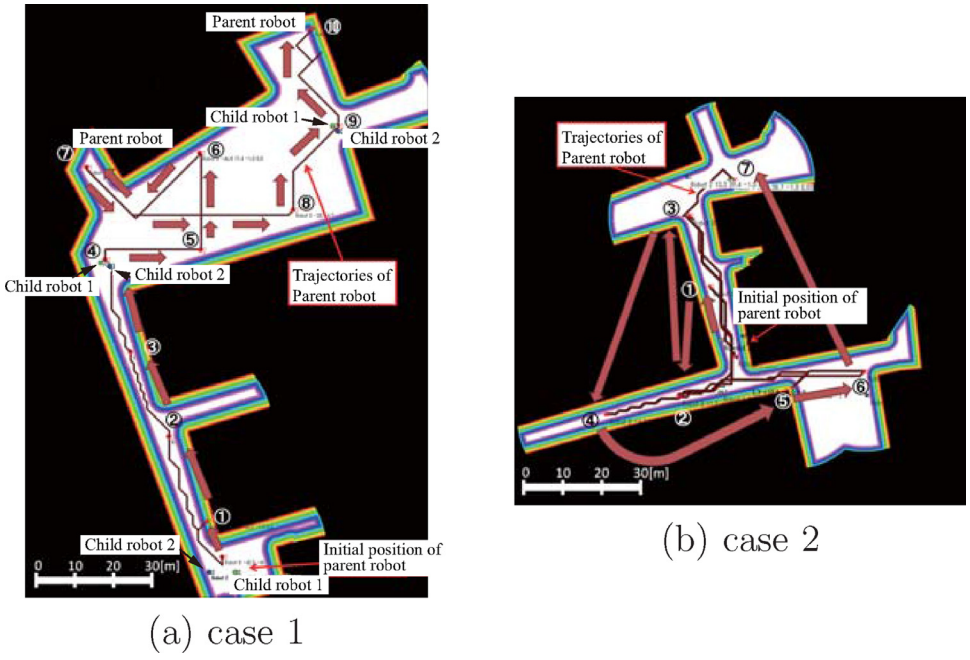

Fig. 23. Trajectories of parent and child robots.

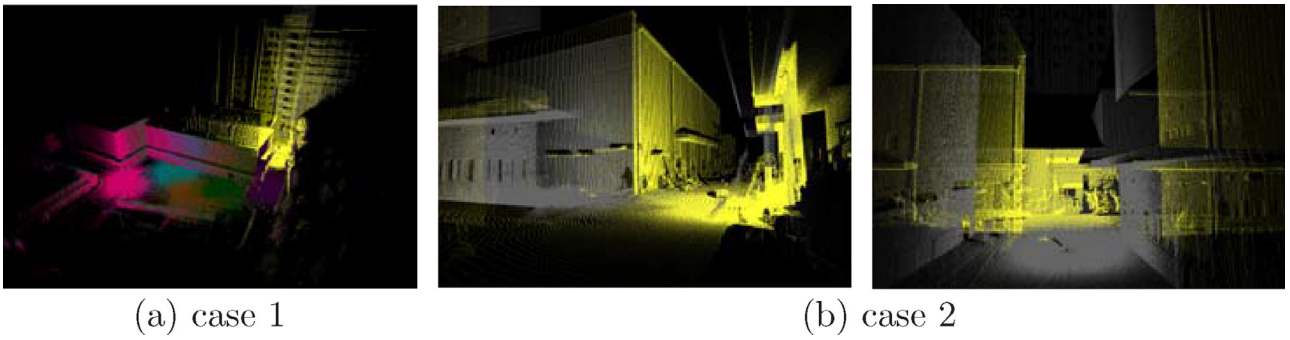

Fig. 24. 3D models obtained by CPS-VII.

Please cite this article as: R. Kurazume et al., Automatic large-scale three dimensional modeling using cooperative multiple robots, Computer Vision and Image Understanding (2016), http://dx.doi.org/10.1016/j.cviu.2016.05.008

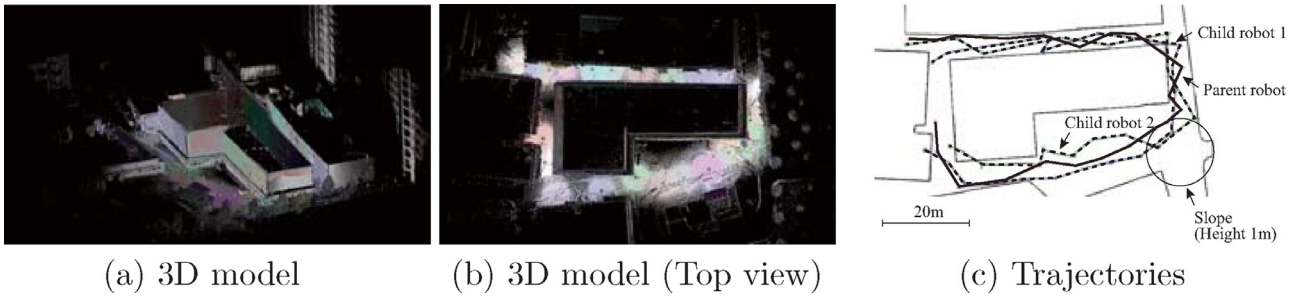

Fig. 25. 3D models and trajectories of parent and child robots.

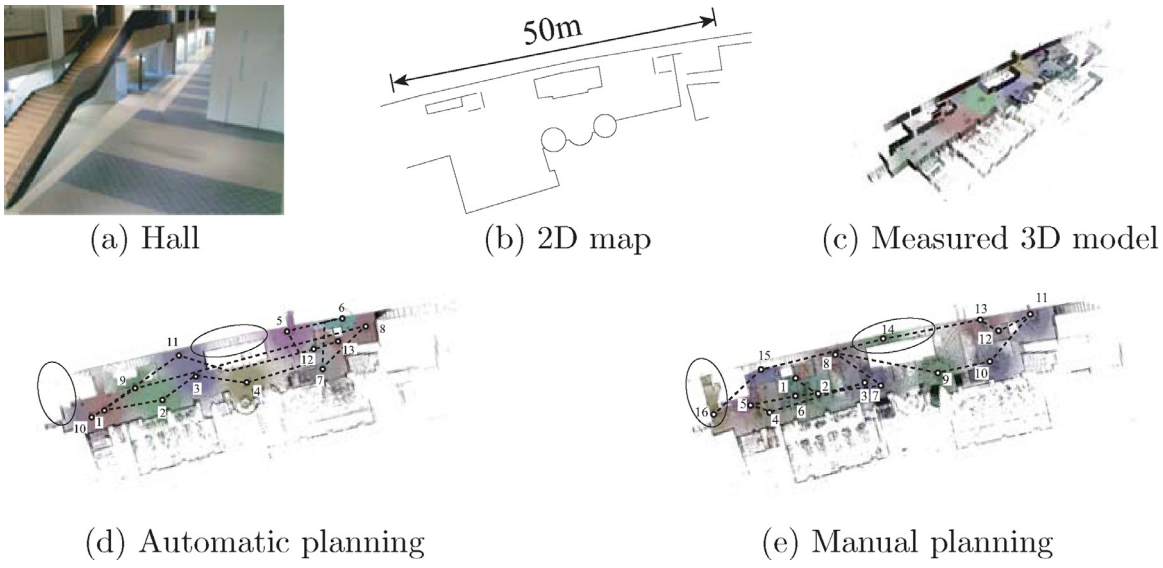

Fig. 26. Examples of trajectories planned by automatic and manual methods.

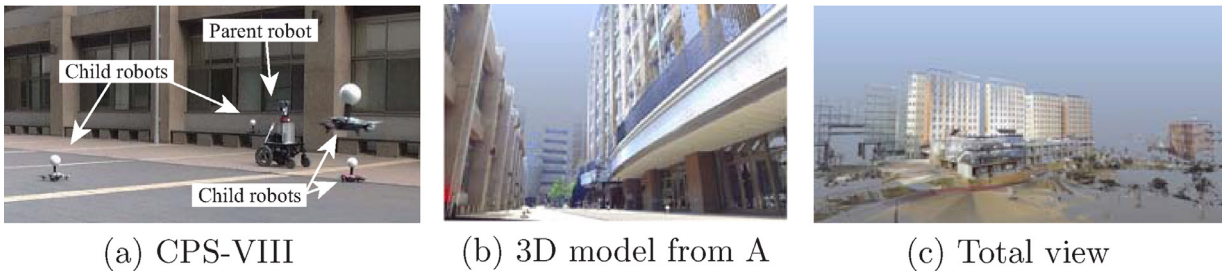

Fig. 27. CPS-VIII and 3D model of buildings.

Table 1
Comparison of positioning error variances for Maps A, B, and C after the parent robot moves nine times [mm^2].

	(a) Random	(b) Angle & distance	(c) Angle	(d) Distance
Map A	500.0	112.3	94.0	159.3
Map B	46.5	43.6	43.7	165.2
Map C	254.2	45.3	47.2	145.8

expected measurement areas become large when the parent robot position is planned by Eq. (1).

An example of the accumulated error for each condition for Map A is shown in Fig. 19. It is clearly seen that the errors are accumulated greatly in conditions (a) and (d), which did not consider the relative angles between child robots. On the other hand, conditions (b) and (c) can suppress error accumulation by selecting the positions where the relative angle becomes 90 degrees. Table 1 shows the error variance of the ninth movement after the parent robot starts to move from the star in Fig. 13. From this table, we can conclude the following.

1. Conditions (b) and (c), which considered the relative angles between child robots, tend to suppress error accumulation in all maps.
2. Condition (d), which considered the relative distance between parent and child robots only, shows large error accumulation in all maps.
3. Random selection of the child robot position induces a large variation of error accumulation and the accuracy tends to be unstable.

5.2. Comparison of CPS-VII and CPS-VIII

Finally, we compared the measurement efficiencies of CPS-VII and CPS-VIII. In the simulation, we set $\alpha = 0.01$, $\beta = 0.001$,

Please cite this article as: R. Kurazume et al., Automatic large-scale three dimensional modeling using cooperative multiple robots, Computer Vision and Image Understanding (2016), http://dx.doi.org/10.1016/j.cviu.2016.05.008

Fig. 28. Route planned by the proposed algorithm.

$\alpha_c = 100$, and $\beta_c = 1$. Fig. 20 shows the comparison of the area coverage rate and the total travel distance of the parent robot for the CPS-VII and CPS-VIII systems.

As shown in Fig. 20, little difference is seen in the area coverage rates between these systems. However, the total travel distance of CPS-VIII is smaller than that of CPS-VII due to the long range of the laser scanner. In addition, since the range sensing and positioning are performed simultaneously for CPS-VIII, the range sensing and movement occur at the same frequency. Thus, the number of movements of CPS-VIII becomes smaller than that of CPS-VII for the same number of measurements.

Fig. 21 shows the results for Map D. We can see that the increasing rate of the area coverage rate against the number of measurements for CPS-VIII is almost the same as that for CPS-VII. However, if we focus on the total travel distance, CPS-VIII finishes the measurement with shorter travel distance than does CPS-VII. This is because the range of the measurement for CPS-VIII is longer than that for CPS-VII, and CPS-VIII can scan a wider area from distant positions. The increasing rates of the area coverage rates against the travel distance of 1 m, that is, the efficiency of the movement, is 0.159 %/m for CPS-VII and 0.344 %/m for CPS-VIII. Additionally, the number of movements when the area coverage rate becomes larger than 90 % is 15 for CPS-VII and 8 for CPS-VIII. Therefore, we can conclude that CPS-VIII is more efficient than CPS-VII.

5.3. Outdoor experiment in a real environment by CPS-VII

We conducted an actual experiment in an outdoor environment by using the CPS-VII system consisting of a parent robot and two child robots, as shown in Fig. 2. The parent robot is equipped with a total station (TOPCON, GPT-9005A, Table 2), auto-leveling system (Risumu, AS-21), 1-axis laser scanner (SICK, LMS-511, Table 3), 1-axis rotation table (Chuo-Seiki, ARS-136-HP), and 2-axis inclinometer (Applied Geomechanics Inc., MD-900-TS). Fig. 22 shows the measured environment and CPS-VII during the experiments.

Fig. 23 shows the planned trajectories of the parent and child robots for two different areas. The arrows and the numbers in these figures indicate the moving direction and the number of movement of the parent robot, respectively. In Fig. 23(a), the parent robot started the measurements from the initial position (bottom), moved along a narrow road, turned right, and entered into an open area. The child robots changed their positions at fourth and ninth movements of the parent robot. On the other hand, in

Table 2
Specification of GPT-9005A (TOPCON).

Range	1.3–3000 m
Angular resolution	0.5″/1″
Accuracy (distance)	±2 mm + 2 ppm × Distance
Accuracy (angle)	1″

Table 3
Specification of LMS-511 (SICK).

Range	0.7–80 m
Angular resolution	0.25°
Accuracy (distance)	± 25 mm– ± 35 mm

Fig. 29. Comparison with photos and 3D models captured from points B, C, D, and E in Fig. 28.

Fig. 23(b), the parent robot repeated the measurements at the upper and the lower areas while moving along a center road. The subgoal retrieval was performed at seventh movement in this case. The child robot 1 moved at second, third, and seventh movements of the parent robot, and the child robot 2 moved at second, fourth, sixth, and seventh movement of the parent robot. Finally, the 3D model can be obtained automatically as shown in Fig. 24.

In addition, the 3D model obtained after the robots moved around the building is shown in Fig. 25(a) and (b), and the planned trajectories for all the robots are illustrated in Fig. 25(c). The parent and child robots started to move from the initial position (top-left position in Fig. 25(c)) and their trajectories were planned automatically, as shown by the dotted lines. In this experiment, the parent robot scanned 26 times around the building and obtained 9.85 million points.

5.4. Comparison with manual planning method

We compared the scanning efficiency between the proposed automatic planning method and the manual planning method through the measurements of a large hall shown in Fig. 26(a) and (b). The 3D model measured by the proposed automatic method is shown in Fig. 26(c) and trajectories for the proposed method and the manual method are shown in Fig. 26(d) and (e), respectively. The number of measurements is 13 for the proposed method whereas it is 16 for the manual method. By the automatic planning, two corridors (indicated by circles) were not measured sufficiently, since the system judged these corridors are too narrow for the robots to pass through, and the robot did not scan from positions in these areas as No.14 and 16 in Fig. 26(e) planned by the manual method. From these trajectories, we can say that the proposed automatic planning method performed the measurements more uniformly than the manual planning method.

5.5. Outdoor experiment in a real environment by CPS-VIII

We applied the proposed automatic planning algorithm to CPS-VIII, consisting of the parent robot and four quadcopters, and scanned a large building. CPS-VIII during measurements and the obtained 3D model are shown in Fig. 27. We can see that a quite precise 3D model is obtained. The robots moved the trajectories determined by the proposed algorithm, as shown in Fig. 28. While the robots moved around the building, the parent robot scanned 14 times. The total travel distance of the parent robot was 270.1 m.

In addition, we evaluated the accuracy of the positioning and the 3D model by comparing the positions of six corners of the 3D model. The positions are the circles shown in Fig. 28 at the 1st and 14th scannings. The average error of these six corners is 23.1 mm, which is 0.0085 % of the total travel distance (270.1 m). This result shows clearly that the proposed CPS-SLAM performs quite accurate 3D modeling as compared to conventional SLAM systems. One of

Please cite this article as: R. Kurazume et al., Automatic large-scale three dimensional modeling using cooperative multiple robots, Computer Vision and Image Understanding (2016), http://dx.doi.org/10.1016/j.cviu.2016.05.008

the reasons why the accuracy is improved as compared with CPS-VII is that the total station and the laser scanner in CPS-VII are integrated and replaced by a single laser scanner, and thus no calibration error exists between the sensors in CPS-VIII. Fig. 29 shows the 3D model with some photos taken from the same positions.

Note that we can apply ICP to the measured point data, as we did in Kurazume et al. (2009). However, we think that absolute accuracy cannot be guaranteed for aligned data because each data value is aligned so that the total relative error is minimized. In the worst case, the obtained 3D model differs from the real shape if the point correspondences are not determined appropriately. On the other hand, the proposed measurement system can guarantee the accuracy level in terms of absolute accuracy, and thus it is quite useful for real applications, such as field robot navigation or 3D shape measurements in construction sites.

6. Conclusions

This paper proposes an automatic planning technique for efficient laser measurement for the CPS-SLAM system, which realizes accurate 3D modeling by using multiple robots and a laser scanner. By planning a proper scanning strategy that satisfies several conditions to validate the CPS motion, efficient and accurate laser scanning can be performed even in a large-scale environment. The proposed technique plans a reliable scanning trajectory by using subgoal retrieval and a Visibility Graph, and the minimization of error accumulation is also realized by considering the relative robot positions. This technique is based on the frontier-based approach (Yamauchi, 1997) and the robot moves to and scans from the frontiers if the frontiers exist in the obtained map and these areas are reachable. Therefore, the robots will cover a whole accessible area assuming perfect sensors and perfect motor control (Yamauchi, 1997). The validity of the proposed technique is verified through computer simulations and actual experiments in an outdoor environment by two types of CPS-SLAM systems. Although this paper dealt with planning in 2D space, the proposed algorithm can be applied to planning in 3D space by considering mutual visibilities and newly scanned areas in 3D.

Acknowledgment

The present study was supported in part by a Grant-in-Aid for Scientific Research (A) (26249029).

References

Aggarwal, A., 1984. The Art Gallery Theorem: Its Variations, Applications, and Algorithmic Aspects. Johns Hopkins University Ph.d. thesis.
Aloimonos, Y., (Ed.) 2013. Active Perception. Psychology Press.
Atanasov, N., Ny, J.L., Daniilidis, K., Pappas, G.J., 2015. Decentralized active information acquisition: theory and application to multi-robot SLAM. In: Proceedings of IEEE International Conference on Robotics and Automation (ICRA), pp. 3775–4782.
Aurenhammer, F., 1991. Voronoi diagrams, a survey of a fundamental geometric data structure. ACM Comput. Surv. (CSUR) 23 (3), 345–405.
Bajcsy, R., 1988. Active perception. Proc. IEEE 76 (8), 966–1005.
de Berg, M., Cheong, O., van Kreveld, M., Overmars, M., 1997. Computational Geometry: Algorithms and Applications. Springer.
Carlone, L., Du, J., Ng, M.K., Bona, B., Indri, M., 2010. An application of Kullback-Leibler divergence to active SLAM and exploration with particle filters. In: Proceedings of IEEE/RSJ International Conference on Intelligent Robots and Systems (IROS), pp. 287–293.
Carrillo, H., Latif, Y., Rodriguez-Arevalo, M.L., Neira, J., Castellanos, J.A., 2015. On the monotonicity of optimality criteria during exploration in active SLAM. In: Proceedings of IEEE International Conference on Robotics and Automation (ICRA), pp. 1476–1483.
Chen, S.Y., Li, Y.F., 2004. Automatic sensor placement for model-based robot vision. IEEE Trans. Syst. Man Cybern. Part B 34 (1), 393–408.
Chen, S.Y., Li, Y.F., 2005. Vision sensor planning for 3-D model acquisition. IEEE Trans. Syst. Man Cybern. Part B 35 (5), 894–904.
Geng, L., Zhang, Y., Wang, J., Fuh, J.Y., Teo, S., 2013. Mission planning of autonomous UAVs for urban surveillance with evolutionary algorithms. In: Proceedings of 10th IEEE International Conference on Control and Automation (ICCA), pp. 828–833.
Jeong, Y., Kurazume, R., Pyo, Y., Iwashita, Y., Hasegawa, T., 2012. High-precision three-dimensional laser measurement system by cooperative multiple mobile robots. In: Proceedings of IEEE/SICE International Symposium on System Integration (SII), pp. 198–205.
Konolige, K., Limketkai, B., Schulz, D., Stewart, B., Fox, D., Ko, J., 2006. Distributed multirobot exploration and mapping. Proc. IEEE 94 (7), 1325–1339.
Kurazume, R., Hirose, S., 1998. Study on cooperative positioning system - optimum moving strategies for CPS-III. In: Proceedings of IEEE International Conference on Robotics and Automation (ICRA), vol. 4, pp. 2896–2903.
Kurazume, R., Nagata, S., Hirose, S., 1994. Cooperative positioning with multiple robots. In: Proceedings of IEEE International Conference on Robotics and Automation (ICRA), Vol. 2, pp. 1250–1257.
Kurazume, R., Noda, Y., Tobata, Y., Lingemann, K., Iwashita, Y., Hasegawa, T., 2009. Laser-based geometric modeling using cooperative multiple mobile robots. In: Proceedings of IEEE International Conference on Robotics and Automation (ICRA), pp. 3200–3205.
Leung, C., Huang, S., Dissanayake, G., 2006. Active SLAM using model predictive control and attractor based exploration. In: Proceedings of IEEE/RSJ International Conference on Intelligent Robots and Systems (IROS), pp. 5026–5031.
Li, Y.F., Liu, Z.G., 2005. Information entropy-based viewpoint planning for 3-D object reconstruction. IEEE Trans. Robot. 21 (3), 324–337.
Marchand, E., Chaumette, F., 1997. Active sensor placement for complete scene reconstruction and exploration. In: Proceedings of IEEE International Conference on Robotics and Automation (ICRA), pp. 743–750.
Mavrinac, A., Chen, X., 2013. Modeling coverage in camera networks: A survey. Int. J. Comput. Vis. 101 (1), 205–226.
Newman, T.S., Jain, A.K., 1995. A survey of automated visual inspection. Comput. Vision Image Understand. 61 (2), 231–262.
Nilsson, U., Ogren, P., Thunberg, J., 2008. Optimal positioning of surveillance UGVs. In: Proceedings of IEEE/RSJ International Conference on Intelligent Robots and Systems (IROS), pp. 2539–2544.
Okamoto, J., Milanova, M., Bueker, U., 1998. Active perception system for recognition of 3d objects in image sequences. In: 5th International Workshop on Advanced Motion Control, pp. 700–705.
O'Rourke, J., 1987. Art Gallery Theorems and Algorithms. Oxford University Press.
Oshima, S., Nagakura, S., Jeong, Y., Iwashita, Y., Kurazume, R., 2015. Automatic planning of laser measurements for a large-scale environment using CPS-SLAM system. In: Proceedings of IEEE/RSJ International Conference on Intelligent Robots and Systems (IROS), pp. 4437–4444.
Papadopoulos-Orfanos, D., Schmitt, F., 1997. Automatic 3-D digitization using a laser rangefinder with a small field of view. In: Proceedings of International Conference on Recent Advances in 3-D Digital Imaging and Modeling, pp. 60–67.
Prieto, F., Redarce, T., Boulanger, P., Lepage, R., 1999. CAD-based range sensor placement for optimum 3D data acquisition. In: Proceedings of Second International Conference on 3-D Digital Imaging and Modeling, pp. 128–137.
Robin, C., Lacroix, S., 2016. Multi-robot target detection and tracking: taxonomy and survey. Auton. Robots 40 (4), 729–760.
Scott, W.R., Roth, G., Rivest, J.-F., 2001. View planning with a registration constraint. In: Proceedings of Third International Conference on 3-D Digital Imaging and Modeling, pp. 127–134.
Sim, R., 2005. Stable exploration for bearings-only SLAM. In: Proceedings of IEEE International Conference on Robotics and Automation (ICRA), pp. 2411–2416.
Stachniss, C., Hahnel, D., Burgard, W., 2004. Exploration with active loop closing for FastSLAM. In: Proceedings of IEEE/RSJ International Conference on Intelligent Robots and Systems (IROS), pp. 1505–1510.
Stamos, I., Allen, P.K., 1998. Interactive sensor planning. In: Proceedings of the IEEE Computer Society Conference on Computer Vision and Pattern Recognition, pp. 489–494.
Tarabanis, K.A., Allen, P.K., Tsai, R.Y., 1995. A survey of sensor planning in computer vision. IEEE Trans. Robotics Autom. RA-11 (1), 86–104.
Tobata, Y., Kurazume, R., Noda, Y., Lingemann, K., Iwashita, Y., Hasegawa, T., 2012. Laser-based geometrical modeling of large-scale architectural structures using co-operative multiple robots. Auton. Robot 32 (1), 49–62.
Tokekar, P., Isler, V., 2014. Polygon guarding with orientation. In: Proceedings of IEEE International Conference on Robotics and Automation (ICRA), pp. 1014–1019.
Topcuoglu, H.R., Ermis, M., Sifyan, M., 2011. Positioning and utilizing sensors on a 3-d terrain -part i theory and modeling. IEEE Trans. Syst. Man Cybern. Part C 41 (3), 376–382.
Yamauchi, B., 1997. A frontier-based approach for autonomous exploration. In: Proceedings of IEEE International Symposium on Computational Intelligence in Robotics and Automation, pp. 146–151.
Zha, H., Morooka, K., Hasegawa, T., Nagata, T., 1997. Active modeling of 3-D objects: Planning on the next best pose (NBP) for acquiring range images. In: Proceedings of International Conference on Recent Advances 3-D Digital Imaging Modeling, pp. 68–75.

Please cite this article as: R. Kurazume et al., Automatic large-scale three dimensional modeling using cooperative multiple robots, Computer Vision and Image Understanding (2016), http://dx.doi.org/10.1016/j.cviu.2016.05.008